Available online at www.sciencedirect.com

SciVerse ScienceDirect

Polar Science 7 (2013) 136–148

http://ees.elsevier.com/polar/

Characteristics of evapotranspiration from a permafrost black spruce forest in interior Alaska

Taro Nakai [a,*], Yongwon Kim [a], Robert C. Busey [a], Rikie Suzuki [b], Shin Nagai [b], Hideki Kobayashi [b], Hotaek Park [c], Konosuke Sugiura [c,a], Akihiko Ito [d,b]

[a] *International Arctic Research Center, University of Alaska Fairbanks, 930 Koyukuk Drive, Fairbanks, AK 99775-7340, USA*
[b] *Research Institute for Global Change, Japan Agency for Marine-Earth Science and Technology, 3173-25 Showa-machi, Kanazawa-ku, Yokohama, Kanagawa 236-0001, Japan*
[c] *Research Institute for Global Change, Japan Agency for Marine-Earth Science and Technology, 2-15 Natsushima-Cho, Yokosuka, Kanagawa 237-0061, Japan*
[d] *Center for Global Environmental Research, National Institute for Environmental Studies, Onogawa 16-2, Tsukuba, Ibaraki 305-8506, Japan*

Received 1 September 2012; revised 10 March 2013; accepted 15 March 2013
Available online 27 March 2013

Abstract

Here, the year 2011 characteristics of evapotranspiration and the energy budget of a black spruce forest underlain by permafrost in interior Alaska were explored. Energy balance was nearly closed during summer, and the mean value of the daily energy balance ratio (the ratio of turbulent energy fluxes to available energy) from June to August was 1.00, though a large energy balance deficit was observed in the spring. Such a deficit was explained partly by the energy consumed by snowmelt. Ground heat flux played an important role in the energy balance, explaining 26.5% of net radiation during summer. The mean daily evapotranspiration of this forest during summer was 1.37 mm day^{-1} – considered typical for boreal forests. The annual evapotranspiration and sublimation yielded 207.3 mm year^{-1}, a value much smaller than the annual precipitation. Sublimation accounted for 8.8% (18.2 mm year^{-1}) of the annual evapotranspiration and sublimation; thus, the sublimation is not negligible in the annual water balance in boreal forests. The daytime average decoupling coefficient was very small, and the mean value was 0.05 during summer. Thus, evapotranspiration from this forest was mostly explained by the component from the dryness of the air, resulting from the aerodynamically rough surface of this forest.

Keywords: Evapotranspiration; Black spruce; Permafrost; Energy balance; Sublimation; Decoupling coefficient

1. Introduction

In recent decades, the importance of the Arctic and Subarctic regions upon the changing climate has been emphasized. The climate of the Arctic warmed significantly over the last 30 years of the 20th century (Serreze et al., 2000), and climate change at high latitudes – including in boreal forest regions – is expected to be the greatest and most rapid on Earth (IPCC, 2001). In addition, related changes in terrestrial ecosystems and hydrological processes in the Arctic region have also been reported (e.g. Hinzman et al.,

* Corresponding author. Tel.: +1 907 474 7254; fax: +1 907 474 2691.
E-mail address: taro.nakai@gmail.com (T. Nakai).

1873-9652
http://dx.doi.org/10.1016/j.polar.2013.03.003

2005). And since boreal forests occupy about 17% of the vegetated surface of the globe (e.g. Whittaker, 1975; Jarvis et al., 1997; Smith et al., 2001), understanding the characteristics of this biome with respect to energy, water, and carbon cycling is important to reducing uncertainty when predicting future climate change in the Arctic and Subarctic regions.

Black spruce is one of the most abundant forest types in North America, occupying approximately 44% of the forest cover of interior Alaska (Viereck et al., 1986). This species dominates north-facing slopes and poorly drained forested lowlands, and is usually associated with permafrost (Chapin et al., 2006). The floor of such black spruce forests is covered by thick moss layers, which insulate mineral soil from extremes such as high temperatures in summer, and which maintain the high permafrost table (Van Cleve and Dyrness, 1983). Iwata et al. (2012) have noted that the presence of ice-rich permafrost under the black spruce forest is important to the retention of sustainable water resources. Underlain by permafrost, the black spruce forest is therefore thought to play an important role in the hydrological processes of interior Alaska and (Sub)Arctic regions. Though many flux measurement studies have been conducted in black spruce forests (e.g. Jarvis et al., 1997; Liu et al., 2005), Iwata et al. (2012) was the only study that dealt with the evapotranspiration from a black spruce forest underlain by permafrost. Thus, it is still important to explore the characteristics of evapotranspiration from permafrost black spruce forests at different sites. Especially since Iwata et al. (2012) discussed the energy balance using half-hourly data, the energy balance of daily data or longer time scales is still unknown, which may be important in discussing the contribution of ground heat flux.

Boreal forest evapotranspiration has been measured at many sites – in Siberia (e.g. Kelliher et al., 1997; Ohta et al., 2001; Matsumoto et al., 2008a; Ohta et al., 2008) and Canada (e.g. Amiro and Wuschke, 1987; Baldocchi et al., 1997; Jarvis et al., 1997), as well as in Alaska (e.g. Iwata et al., 2012). However, a great deal of these studies have dealt with evapotranspiration during the snow-free period, and thus the annual water vapor flux, including sublimation in winter and how sublimation contributes to the annual evapotranspiration and sublimation, is still unclear. Though Iwata et al. (2012) showed the seasonal change in the monthly water vapor flux, including winter, they did not provide the actual values of the winter water vapor flux. Even though sublimation from snow has been observed by eddy covariance method in the relatively warmer forests of Colorado (Molotch et al., 2007) and Idaho (Reba et al., 2012) in the USA and Hokkaido in Japan (Nakai et al., 1999), observational studies on sublimation in boreal forests are rarely found. Further, the observational sublimation studies that do exist have been limited in winter, and thus the contribution of sublimation to the annual total water vapor flux in boreal forests is still unclear.

The objective of this study, then, was to explore the characteristics of evapotranspiration from a permafrost black spruce forest in interior Alaska, in view of energy balance, daily and annual evapotranspiration and sublimation, and the relationship and coupling of plants to the atmosphere.

2. Materials and methods

2.1. Study site

Observations were conducted at the site of a black spruce forest at the Poker Flat Research Range (PFRR) of the University of Alaska Fairbanks (65°07′24.4″ N, 147°29′15.2″ W), located in interior Alaska (Fig. 1). This site was established as a supersite of the JAMSTEC-IARC Collaboration Study (JICS) in 2010 (Sugiura et al., 2011). The dominant overstory tree species in this forest is black spruce (*Picea mariana*), with the forest floor nearly covered by a moss layer of rusty peat moss (*Sphagnum fuscum*) and splendid feather moss (*Hylocomium splendens*), and partly covered by tussock with cotton-grass (*Eriophorum vaginatum*). The understory is dominated by low shrubs and herbs such as Labrador tea (*Ledum groenlandicum*), bog bilberry (*Vaccinium uliginosum*), dwarf birch (*Betula nana*), and cloudberry (*Rubus chamaemorus*). This lowland black spruce forest is considered a bog forest (e.g. Viereck et al., 1986; Billings, 1987). Black spruce trees are distributed heterogeneously, and some patchy open areas existed at the time of study.

A tree survey of this forest was conducted in July 2010, and tree height, diameter at breast height (DBH), and the location of the 357 samples taller than 1.3 m were measured within a 30 m by 30 m plot. Eight samples out of 357 trees were speckled alder (*Alnus rugosa*); all others were black spruce. Table 1 shows the characteristics of this forest, and Fig. 2 shows the distributions of tree height frequency and cumulative basal area against tree height. By fitting the Richards function to the plot of cumulative basal area against tree height, CuBI (cumulative basal area inflection) height (Nakai et al., 2010) was calculated as 2.91 m (Fig. 2). This height corresponds to the tree height

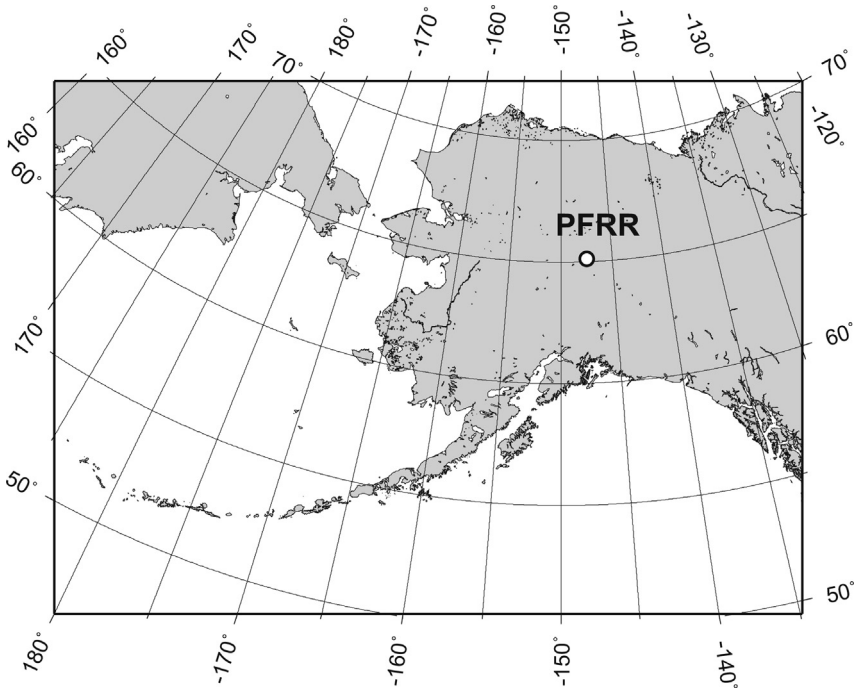

Fig. 1. Map of the study site at the Poker Flat Research Range (PFRR), University of Alaska Fairbanks, located in interior Alaska.

class, within which the subtotal of the basal area is the largest by definition (Nakai et al., 2010). In this forest, CuBI height was slightly higher than the arithmetic mean height (2.44 m), and much lower than the maximum tree height (6.4 m) (Table 1). This black spruce forest consisted mainly of short trees; trees shorter than CuBI height (2.91 m) accounted for 74.8%, whereas trees taller than 4.0 m occupied 11.2% of the total. CuBI height of this forest, therefore, was considered representative of the abundant short trees.

The leaf area index (LAI) of overstory black spruce was 0.73, measured on 24 September 2011 using an LAI-2000 (LI-COR, Lincoln, Nebraska, USA); the effect of leaf clumping was considered. The ground surface was covered with a thick moss layer. According to the soil profile survey conducted on 23 September 2010, the layer of 0–14 cm surface depth was the moss layer. The layer of 14–25 cm surface depth was an undecomposed organic layer, and at 25–39 cm was a decomposed organic layer. The layer

Table 1
Characteristics of overstory black spruce trees taller than 1.3 m at the observation site, according to the tree survey conducted in July of 2010.

Characteristic	Data
Stand density, trees ha^{-1}	3967
Maximum tree height, m	6.4
Average tree height, m	2.44
CuBI height (Nakai et al., 2010), m	2.91
Maximum DBH, cm	8.6
Basal area, m^2 ha^{-1}	2.6

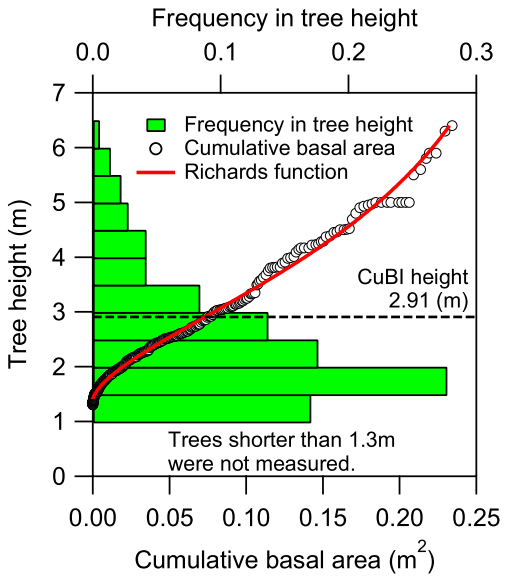

Fig. 2. Distribution of tree height frequency (bar graph) and cumulative basal area (open circle) against tree height of samples taller than 1.3 m, together with the CuBI (cumulative basal area inflection) height (Nakai et al., 2010) as a representative canopy height of this forest.

below 39 cm was silty and cryoturbated, and the active layer depth was at 43 cm. This thawing depth was considered the deepest of the year; soil deeper than 43 cm was permafrost.

2.2. Measurements

A 17-m tower was built at this site in order to measure eddy covariance fluxes and meteorological variables. Observed items, measurement height (depth), and instruments are listed in Table 2. Observations began in October 2010, and the ensuing year-round data from 2011 was used in this study. Hereafter, subscripts T and F indicate radiation measurements at the tower (16 m in height) and on the forest floor (1.3 m above the ground), respectively.

Net radiation at the tower R_{nT} (W m^{-2}) and the forest floor R_{nF} (W m^{-2}) were calculated from downward/upward short-wave radiation and downward/upward long-wave radiations measured independently by CNR4 (Kipp & Zonen, the Netherlands). For example, R_{nT} was calculated as follows.

$$R_{nT} = S_{dT} - S_{uT} + L_{dT} - L_{uT}, \quad (1)$$

where S_{dT} and S_{uT} (W m^{-2}) are downward and upward short-wave radiation, and L_{dT} and L_{uT} (W m^{-2}) are downward and upward long-wave radiation, respectively. Ground heat flux G (W m^{-2}) was measured using a heat flux plate (HFP01SC, Hukseflux, The Netherlands) at 8-cm depth in the moss layer at two points, and the average of these measurements was used. Mean air temperature and relative humidity were measured at eight levels (Table 2) by an HMP155 (Vaisala, Finland) installed in a ventilated double-walled tube.

Soil moisture was measured by water content reflectometry (WCR) instruments (CS616, Campbell Sci., USA). To convert the WCR probe output period into volumetric soil water content (VSWC), the empirical calibration function of Bourgeau-Chavez et al. (2012) was employed for the organic layer (5 cm–30 cm), and that of Campbell Scientific, Inc. (2006) was applied for mineral soil (40 cm). Though Bourgeau-Chavez et al. (2012) provided calibration functions for each soil horizon (i.e., dead moss, upper duff, lower duff, and mineral soil), some of them resulted in calculations of greater than 100% VSWC in this study, and the general function was adopted for the organic layer from 5 cm to 30 cm depth, also provided by Bourgeau-Chavez et al. (2012).

Sensible heat flux H (W m^{-2}) and latent heat flux λE (W m^{-2}) measurements obtained from the tower at 11.0 m in height were used in this study (Table 2), where λE is a product of water vapor flux E (kg m^{-2} s^{-1} = mm s^{-1}) and the latent heat of vaporization or sublimation λ (J kg^{-1}). These fluxes were measured by eddy covariance technique, using a WindMaster Pro ultrasonic anemometer (Gill Instruments, Lymington, UK) and a LI-7200 enclosed infrared gas analyzer (LI-COR, Lincoln, Nebraska, USA) (Fig. 3). The LI-7200 enables us to measure fluxes with little data loss from precipitation and icing (Burba et al., 2010). When calculating eddy fluxes, angle of attack dependent errors of the WindMaster Pro were corrected according to Nakai and Shimoyama (2012). The mixing ratio of water vapor measured by LI-7200 was used for calculation of latent heat flux (Nakai et al., 2011; Burba et al., 2012). Since the sonic temperature of the WindMaster Pro was corrected

Table 2
List of sensors and measurement height (depth) at the PFRR observation site.

Observed items	Height (depth in negative value) (m)	Sensor
Eddy covariance		
3-D wind velocity, sonic virtual temperature	11.0, 1.85	WindMaster Pro (Gill, UK)
Mixing ratio of water vapor	11.0, 1.85	LI-7200 (LI-COR, USA)
Meteorological measurements		
Net radiation[a]	16.0, 1.3	CNR4 (Kipp & Zonen, The Netherlands)
Photosynthetic active radiation[b]	16.0, 1.3	LI-190 (LI-COR, USA)
Air temperature and relative humidity	16.0, 13.0, 11.0, 9.0, 7.5, 6.0, 4.5, 3.0, 1.5	HMP155 (Vaisala, Finland)
Wind speed	16.0, 13.0, 9.0, 7.5, 6.0, 4.5, 3.0, 1.5	010C (MetOne, USA)
Wind direction	17.0	020C (MetOne, USA)
Soil heat flux	−0.08	HFP01SC (Hukseflux, The Netherlands)
Soil temperature	−0.05, −0.1, −0.2, −0.3, −0.4, −1.0	107 (Campbell Sci., USA)
Volumetric soil water content	−0.05, −0.1, −0.2, −0.3, −0.4	CS616 (Campbell Sci., USA)
Precipitation	On the ground	RS-222A (Ogasawara Keiki, Japan)
Snow depth	1.36, 1.46, 1.59 (3 different points)	SR50A (Campbell Sci., USA)

[a] Upward/downward shortwave radiation and upward/downward longwave radiation were measured separately.
[b] Upward and downward components were measured.

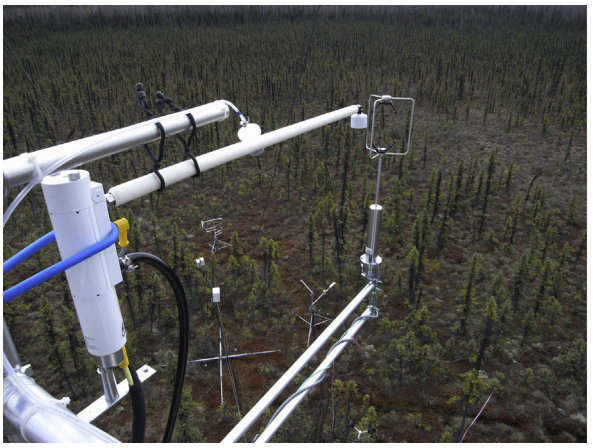

Fig. 3. Photo of the eddy covariance flux measurement system on the tower at 11.0 m above the ground, also showing the land surface condition of a black spruce forest in PFRR.

internally for crosswind, humidity correction of sonic temperature (Schotanus et al., 1983) was applied. Data spikes were removed in accordance with Vickers and Mahrt (1997), and the double coordinate rotation was also used (McMillen, 1988). Frequency response corrections (Moore, 1986) were also applied. The source area of the flux footprint from these sensors was typically about 300 m for 80% contribution in the daytime, according to the footprint model of Kormann and Meixner (2001).

In calculating λE, the latent heat of vaporization λ_v (J kg^{-1}) or latent heat of sublimation λ_s (J kg^{-1}) was used for each half-hourly data entry, depending on the air temperature. If the air temperature T (°C) measured at 11.0 m was positive, λ_v was calculated as follows (Fritschen and Gay, 1979):

$$\lambda_v = 2.50025 \times 10^6 - 2365T. \quad (2)$$

Meanwhile, when T was zero or negative, λ_s was calculated as follows (Fleagle and Businger, 1980; Andreas, 2005):

$$\lambda_s = 2.8341 \times 10^6 - 149T. \quad (3)$$

The quality control and gap filling of the obtained H and λE were made in accordance with Ueyama et al. (2012). In this study, mainly the daily mean values of fluxes were used.

2.3. Energy balance

The energy balance of the whole black spruce forest is expressed as follows:

$$R_{nT} - G = H + \lambda E + J_H + J_E, \quad (4)$$

where J_H and J_E (W m^{-2}) are the sensible heat storage and latent heat storage of the air between the ground surface and the eddy covariance system, respectively. These were calculated using temporal variations in the vertical profiles of air temperature and the mixing ratio of water vapor, respectively.

As has been noted in the literature, the energy balance in Eq. (4) is not usually closed, and the energy balance ratio (EBR) has been used for checking turbulent flux observation, represented as

$$\mathrm{EBR} = \frac{H + \lambda E}{R_{nT} - G - J_H - J_E}. \quad (5)$$

Energy balance deficit (EBD) has also been used for checking energy balance closure (Hendricks Franssen et al., 2010), defined as follows:

$$\mathrm{EBD} = R_{nT} - G - H - \lambda E - J_H - J_E. \quad (6)$$

In this study, the available energy for energy partitioning A (W m^{-2}) was determined as follows:

$$A = R_{nT} - G - J_H - J_E. \quad (7)$$

Also, an evaporative fraction ε (Shuttleworth et al., 1989) was adopted in order to check the relative importance of λE in the energy partitioning, defined as follows:

$$\varepsilon = \frac{\lambda E}{H + \lambda E}. \quad (8)$$

2.4. Calculations of parameters representing characteristics of evapotranspiration

The bulk surface conductance g_s (m s^{-1}) was calculated from the Penman–Monteith equation (Monteith, 1965), using the following form:

$$g_s^{-1} = \left(\frac{\Delta}{\gamma}\frac{H}{\lambda E} - 1\right) g_a^{-1} + \frac{\rho c_p D}{\gamma \lambda E}, \quad (9)$$

in which Δ (hPa K^{-1}) is the rate of change of saturation vapor pressure with temperature; γ (hPa K^{-1}) is the psychrometric constant; ρ (kg m^{-3}) is the moist air density; c_p (J kg^{-1} K^{-1}) is the specific heat of air at constant pressure; and D (hPa) is the saturation vapor pressure deficit. Aerodynamic conductance g_a (m s^{-1}) was estimated from the friction velocity u_* (m s^{-1}) and wind speed U (m s^{-1}), measured by ultrasonic anemometer as follows:

$$g_a = \frac{u_*^2}{U}. \quad (10)$$

McNaughton and Jarvis (1983) rewrote the Penman–Monteith equation in the form

$$\lambda E = \Omega \lambda E_{\mathrm{eq}} + (1-\Omega)\lambda E_{\mathrm{imp}}, \tag{11}$$

where λE_{eq} (W m^{-2}) is the equilibrium evaporation rate, λE_{imp} (W m^{-2}) is the imposed evapotranspiration rate, and Ω is the decoupling coefficient, defined as follows:

$$\lambda E_{\mathrm{eq}} = \frac{\Delta}{\Delta+\gamma} A, \tag{12}$$

$$\lambda E_{imp} = \frac{\rho c_p D}{\gamma} g_s, \tag{13}$$

$$\Omega = \frac{\Delta+\gamma}{\Delta+\gamma(1+g_a/g_s)}. \tag{14}$$

Eq. (11) divides λE into two components: λE_{eq} is evaporation by radiative heating, and λE_{imp} denotes evapotranspiration due to the dryness of the air, without radiative heating. Ω takes the value from 0 to 1 and indicates how evapotranspiration by vegetation is "decoupled" from the saturation deficit of the ambient air, determining the relative importance of λE_{eq} and λE_{imp}.

3. Results and discussion

3.1. Environmental conditions

Fig. 4 shows seasonal variations in meteorological data. At 11.0 m in height in 2011, the lowest temperature during winter was −44.0 °C (21 January), and the highest temperature was 28.8 °C (25 July). Mean annual air temperature was −2.8 °C, and mean temperature over summer (JJA) was 13.5 °C. The temperature increased toward the end of May, and the variation in air temperature was then relatively flat until the end of July. The vapor pressure deficit (VPD) was the highest at the end of May, reaching 30.9 hPa (27 May). The mean value of VPD in summer (JJA) was 5.5 hPa. The variation in soil temperature shows gradual thawing of frozen soil, and the thaw dates at each depth were 15 May (5 cm), 24 May (10 cm), 11 June (20 cm), 25 June (30 cm), and 9 July (40 cm). The freezing of this layer began almost simultaneously from 5 to 8 October. The depth of the active layer was about 50 cm; 100 cm depth was within permafrost, with its temperature negative year-round. The variation in volumetric soil water content (VSWC) shows that the layer below 10 cm was nearly saturated throughout the growing season, believed as due to the presence of

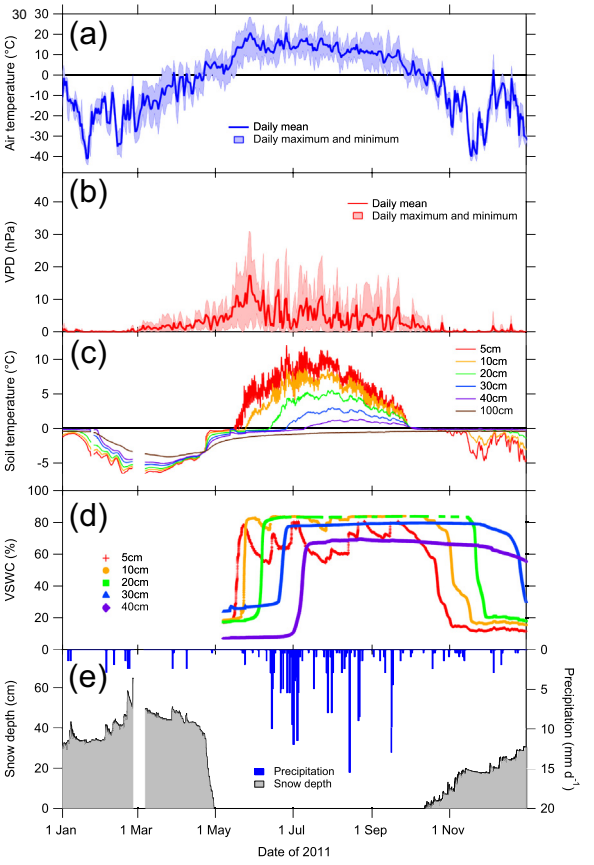

Fig. 4. Seasonal variations in (a) air temperature at the height of 11.0 m, (b) Vapor pressure deficit (VPD) at 11.0 m, (c) Soil temperature, (d) Volumetric soil water content (VSWC), and (e) precipitation (bar graph) and snow depth (shaded graph). Air temperature (a) and VPD (b) are presented with daily average, maximum, and minimum data, and precipitation is shown as daily accumulated values. Other data are 30-min average values.

underlying impermeable permafrost, which prevents downward percolation. Snow depth was at maximum on 25 February (65.0 cm) and reached zero on 29 April. According to the interval of downward fisheye images from the tower top, the snow-covered portion of the ground surface reached less than 50% on 1 May; the day of complete snow disappearance was 5 May. The snow-free period was from 5 May to 12 October. Annual precipitation was 241.5 mm, and the precipitation during the snow-free period was 202.0 mm, according to tipping bucket rain/snow gauge observations. From these results, the precipitation in winter was calculated as 39.5 mm. However, the snow water equivalent at this site was 110.8 mm on 23 March 2011 (number of samples $n = 4$, standard deviation $\sigma = 11.2$ mm) and 114.4 mm on 4 April 2012 ($n = 9$, $\sigma = 11.9$ mm), according to the snow survey. The

precipitation in winter was therefore considered underestimated by about 65% by the tipping bucket gauge. Assuming that the precipitation from snow was 110 mm in 2011, annual precipitation was estimated at 312 mm yr^{-1}.

Fig. 5 shows the radiation environment at this site. Since the site is located at a high latitude, seasonal variation in the daily-mean S_{dT} was significant, ranging from less than 10 W m^{-2} in winter to above 300 W m^{-2} in early summer (Fig. 5(a)). Since snow remained until the beginning of May, a large portion of downward short-wave radiation was reflected by the snow in early spring, even though S_{dT} was relatively large (Fig. 5(a) (b)), and thus seasonal variations in R_{nT} and R_{nF} were skewed and depressed in spring (Fig. 5(c)). Albedo during the growing season (i.e., snow-free period) was almost constant, both at the tower top and on the forest floor (Fig. 5(b)). Mean values of albedo during summer (JJA) were 0.15 at the tower top and 0.11 on the forest floor. Net radiation showed a large difference, meanwhile, between the tower top and forest floor during the growing season (Fig. 5(c)). Note that the distribution of black spruce trees is heterogeneous, and that the radiation measurements on the forest floor can change from site to site. Since radiation sensors were installed relatively close to the dense trees in this study, differences in radiation were emphasized. On cloudy days, when the difference between L_{dT} and L_{uT} was small, the difference between R_{nT} and R_{nF} was also generally small.

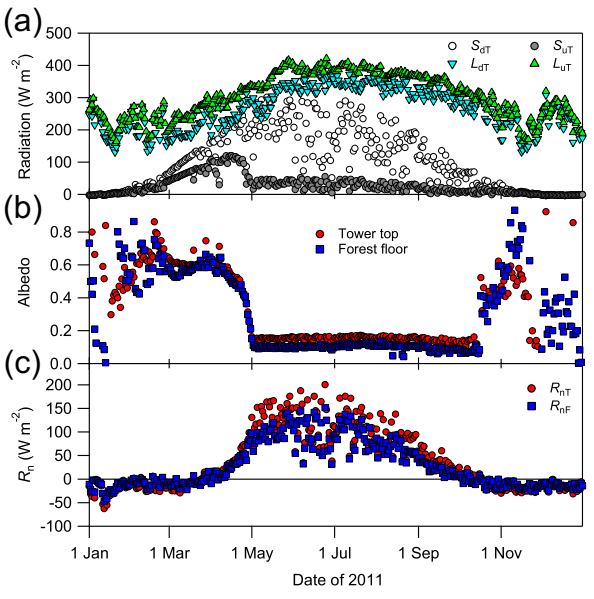

Fig. 5. Seasonal variations in the daily mean values of (a) downward and upward short-wave radiation (S_{dT}, S_{uT}), and downward and upward long-wave radiation (L_{dT}, L_{uT}) at the tower top; (b) Albedo at the tower top and forest floor; and (c) net radiation at the tower top R_{nT} and forest floor R_{nF}.

3.2. Energy balance closure

Fig. 6(a) shows the seasonal variation in energy balance deficit (EBD) from April to September 2011, together with ground heat flux G. The EBD was greatest at the end of April, and remained large through spring before mid-May. Note that G was nearly zero during this period. Otherwise, the variation pattern of EBD seemed to correspond to that of G. Comparing G with $R_{nT} - H - \lambda E - J_H - J_E$ (Fig. 6(b)), G was significantly larger than $R_{nT} - H - \lambda E - J_H - J_E$ during summer, indicating that G was overestimated at

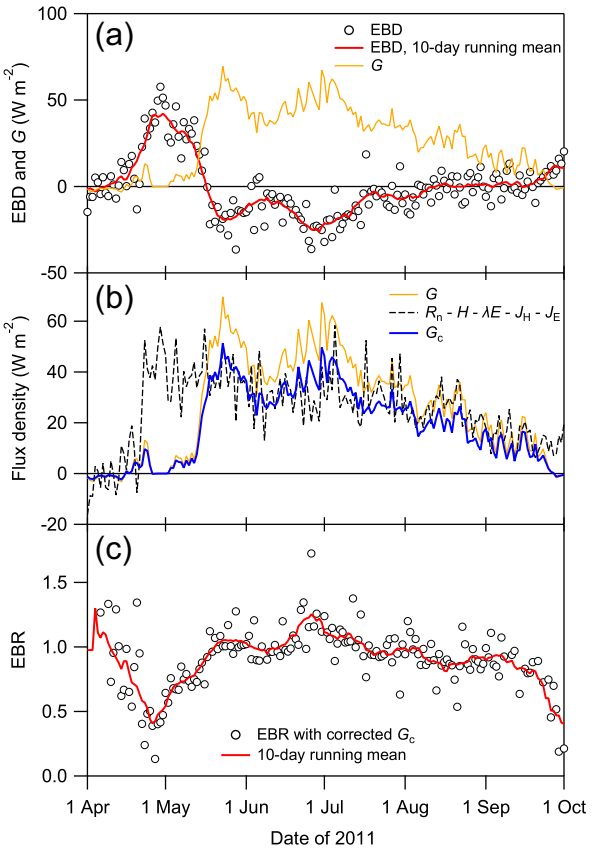

Fig. 6. Seasonal variations in (a) energy balance deficit (EBD) together with G; (b) Uncorrected G and corrected G_c, together with the residual of energy balance other than G (i.e., $R_{nT} - H - \lambda E - J_H - J_E$); and (c) energy balance ratio (EBR). The thick red solid lines denote 10-day running mean values, and others are the daily mean values. (For interpretation of the references to colour in this figure legend, the reader is referred to the web version of this article.)

this site. If G is corrected so that the square sum of EBD is at minimum, using the data from June to September, the corrected ground heat flux G_c was estimated at $G_c = 0.74G$. This correction factor of 0.74 is consistent with the fact that the thermal conductivity of the heat flux plate (HFP01SC) was 0.8 W m^{-1} K^{-1} (Sauer et al., 2008), whereas the maximum thermal conductivity of the *Sphagnum* has been reported to range from 0.5 to 0.6 W m^{-1} K^{-1} at a high volumetric water content (O'Donnell et al., 2009).

By using the corrected G_c, EBR was nearly constant during summer (Fig. 6(c)), and the JJA average of EBR was 1.00. Fig. 7 shows the scatter plot of $H + \lambda E$ against A during JJA. The coefficient of determination R^2 increased by adopting G_c instead of G, and the intercept moved closer to zero. The slope of the regression line was 0.97. Jarvis et al. (1997) also reported a slope of 0.97 as the mean daily energy balance over a black spruce forest in Canada. Therefore, the energy balance in this site was almost closed, and thus H and λE measured by eddy covariance technique were considered reliable. Fig. 8 shows seasonal variations in the daily-mean energy balance components. Clearly, G_c played an important role in energy balance in summer after mid-May and was comparable with H and λE, while storage terms J_H and J_W were negligibly small throughout the year. The large positive value of the daily-mean G_c during this summer period is explained by the fact that the half-hourly G_c was positive (i.e., downward) all day, irrespective of day and night, which was considered correspondent to thawing frozen soil in the active layer. Table 3 shows the annual and summer (JJA) energy balance components. G_c occupied a large portion of energy balance in summer, accounting for 26.5% of R_{nT}. G_c was also

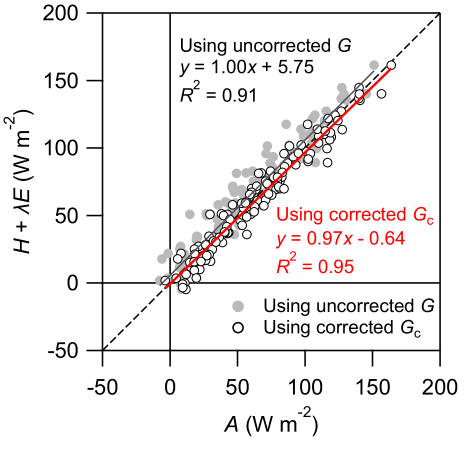

Fig. 7. Scatter plot of the daily mean $H + \lambda E$ against A from June to September, using uncorrected G and corrected G_c.

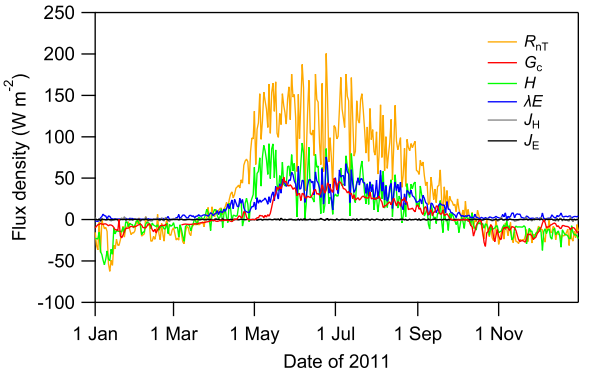

Fig. 8. Seasonal variations in the daily mean values of the components of the energy balance in Eq. (4).

large in the annual energy balance, explaining 13.6% of R_{nT}. H and λE were nearly the same in magnitude over the summer – 35.2% and 37.2% of R_{nT}, respectively – whereas λE was larger than H in the annual energy balance, occupying 44.4% (λE) and 26.6% (H) of R_{nT}. Most importantly, while the EBD in summer was negligibly small (1.1% of R_{nT}), annual EBD was significantly large (16.0% of R_{nT}). One reason for this large EBD is that the latent heat consumed by snowmelt and thaw of frozen soil is not addressed in this energy balance, and thus the energy balance in winter is still unknown.

The large EBD in spring was expected to be used for snow melting. The snow water equivalent of this site was 110.8 mm on 23 March 2011, and the latent heat of fusion to melt this snow was calculated as 37.0 MJ m^{-2} Table 4 shows the energy balance from 23 March to 1 May 2011 (considered as the date when most snow had disappeared). In calculating λE, latent heat of vaporization λ_v was used even at the below freezing point, so as to avoid double counting of the latent heat of fusion. Note that storage terms J_H and J_E were omitted here. The latent heat of fusion calculated above accounted for 33.3% of $R_n - G$. Since EBD during this period was 37.9 MJ m^{-2} (34.1% of $R_n - G$), this EBD was explained by the energy consumed by snowmelt.

On the other hand, however, EBD remained large until mid-May. Considering that G_c was almost zero during this period, this energy may have been consumed by thawing the frozen moss layer above the heat flux plate.

3.3. Evapotranspiration and sublimation

Fig. 9 shows the seasonal variation in the evaporative fraction ε. A clear drop in ε was found in spring

Table 3
Annual and summer (JJA) energy balance components over a black spruce forest in PFRR.

Components	Annual		Summer (JJA)	
	Energy (MJ m^{-2})	Ratio against R_{nT} (%)	Energy (MJ m^{-2})	Ratio against R_{nT} (%)
R_{nT}	1165.8	–	834.2	–
G_c	159.0	13.6	221.4	26.5
H	309.6	26.6	293.3	35.2
λE	517.3	44.4	310.4	37.2
J_H	−0.6	−0.0	−0.1	−0.0
J_E	−0.2	−0.0	−0.0	−0.0
EBD	180.5	15.5	9.3	1.1

from April to mid-May. This is because H was large, whereas λE did not increase enough over this period. Similar phenomena were also found in the Siberian larch forest (Ohta et al., 2001). Other than this period, no clear seasonal variation was found in ε, and it seemed nearly constant. Actually, seasonal variations in H and λE were similar from mid-May to September (Fig. 8). This characteristic is different from that of the larch forest in eastern Siberia, where ε showed a clear seasonal variation, with a peak in summer (Ohta et al., 2008; Matsumoto et al., 2008a). The mean value in summer (JJA) was $\varepsilon = 0.56$. Ohta et al. (2008) reported a value of 0.48 over a dry canopy of larch forest in eastern Siberia for JJA. When ε was classified into zero precipitation and non-zero precipitation days, ε of non-zero precipitation was somewhat larger than that of zero precipitation (Fig. 9). The JJA average of ε of zero precipitation days was 0.50, which was similar to that of Ohta et al. (2008), whereas the JJA average of ε of non-zero precipitation days was 0.63.

Fig. 10(a) shows the seasonal variation in the daily water vapor flux E (i.e., evapotranspiration and sublimation). In summer (JJA), E ranged from 0.40 to 2.65 mm day^{-1}, and the JJA average was 1.37 mm day^{-1}. These results were similar to observations in boreal forests such as the larch forest mentioned in eastern Siberia (1.5–2.5 mm day^{-1}, Kelliher et al., 1997; Ohta et al., 2008), the lichen woodland of black and white spruce in eastern Canada (about 1.5 mm day^{-1} in average, Fitzjarrald and Moore, 1994), and a boreal jack pine forest in central Canada (0.5–2.5 mm day^{-1} Baldocchi et al., 1997). Therefore, daily E at this site was considered typical for boreal forests.

Annual evapotranspiration and sublimation from this black spruce forest was 207.3 mm $year^{-1}$ in 2011 (Fig. 10(b)). This amount represented 85.8% of the annual precipitation of 241.5 mm (rain gauge measurement) and 66.4% of the 312 mm of precipitation during the snow-free period and snow water equivalent. Defining the sublimation as E of when the air temperature at 1.5 m in height was negative in half-hourly data, annual sublimation was estimated at 18.2 mm $year^{-1}$, accounting for 8.8% of the total annual evapotranspiration and sublimation. Therefore, the sublimation in winter is not negligible when

Table 4
Energy balance components and energy consumed by snowmelt from 23 March to 1 May 2011.

Components	Energy (MJ m^{-2})	Energy balance[a] (%)
Energy balance components		
R_{nT}	111.2	–
G_c	0.0	–
H	33.3	29.9
λE	40.0	36.0
Subtotal energy balance	73.3	65.9
EBD	37.9	34.1
Energy consumed by snowmelt		
Latent heat of fusion	37.0	33.3
Total energy balance	110.3	99.2

[a] Percentage against $R_{nT} - G$.

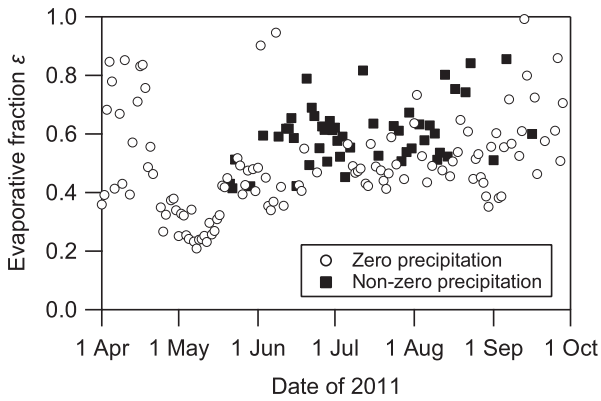

Fig. 9. Seasonal variations in the daily mean evaporative fraction ε on the zero precipitation days and non-zero precipitation days.

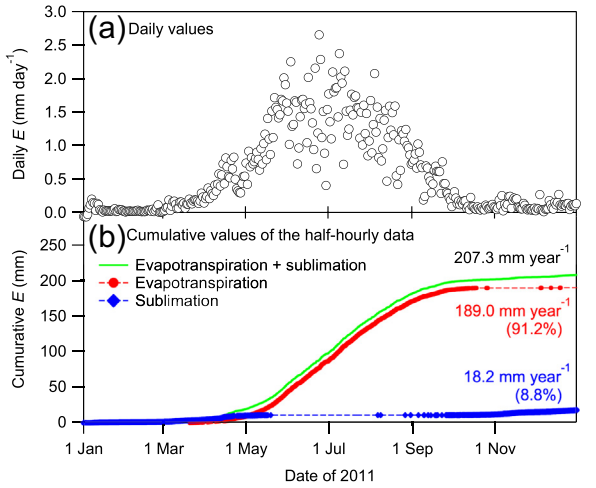

Fig. 10. Seasonal variations in (a) daily evapotranspiration and sublimation E and (b) cumulative evapotranspiration and sublimation E calculated from half-hourly data.

discussing the annual water balance over terrestrial ecosystems in boreal regions.

On the other hand, annual evapotranspiration was estimated at 189.0 mm year^{-1} Iwata et al. (2012) reported that evapotranspiration during the snow-free period ranged from 195.1 mm to 233.6 mm (average of 210.9 mm) over a black spruce forest in Fairbanks, Alaska from 2003 to 2009 − thus the evapotranspiration in this study was relatively small. Even though these two sites are located within a distance of 35 km, the characteristics such as forest floor conditions and topography are quite different from one other. Also, since the observations in the PFRR site began in October 2010, inter-annual variations in the data are still unknown. Detailed comparison studies between these two sites are thus required in the near future.

3.4. Characteristics of evapotranspiration from a permafrost black spruce forest

In this section, the half-hourly data without gap-filling were used for calculations and analyses. Note that the quality control was applied to the data.

Fig. 11 shows the diurnal variations in aerodynamic conductance g_a and bulk surface conductance g_s, in which the ensemble mean (open circle) and standard deviation (error bars) of half-hourly JJA data are presented. Both g_a and g_s showed clear diurnal variation patterns, with a peak in daytime. The ensemble mean g_a ranged from 0.09 to 0.77 m s^{-1}, and generally exceeded 0.5 m s^{-1} in daytime. On the other hand, the maximum of the ensemble mean g_s was 0.008 m s^{-1}.

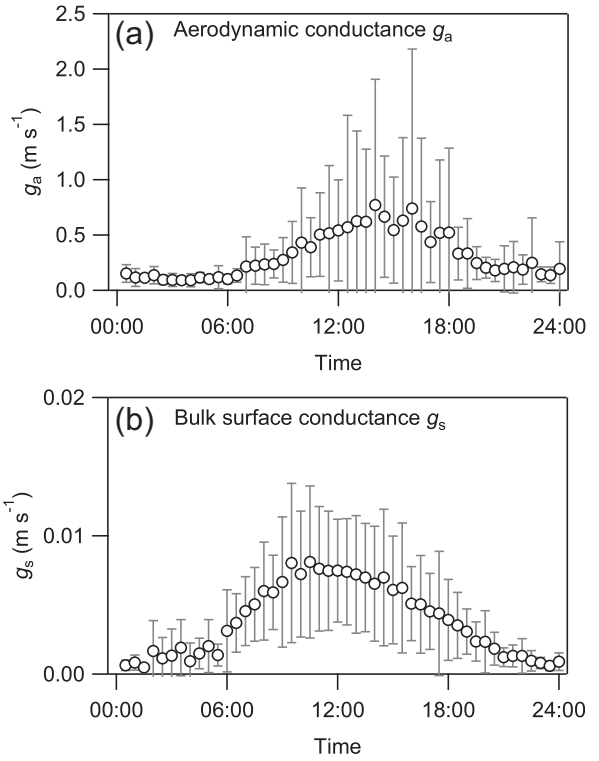

Fig. 11. Diurnal variations in (a) aerodynamic conductance g_a and (b) bulk surface conductance g_s, where the open circles and error bars denote the ensemble mean values and standard deviation of the half-hourly data of JJA, respectively.

Since the diurnal variations in g_a and g_s were significant, the daytime mean values of these data were used to analyze seasonal variations in the characteristics of evapotranspiration. Daytime mean value was calculated from 11:00 to 15:00 AKST, as the solar noon of Fairbanks is roughly 13:00 AKST. Fig. 12 shows seasonal variations in the daytime mean g_s, g_a, decoupling coefficient Ω, as well as the components of Eq. (11). Though g_s was relatively small until the beginning of June, seasonal variations in both g_s and g_a were not significant. Small g_s and large g_a resulted in a very small Ω throughout the growing season; the mean value of Ω in summer (JJA, daytime) was 0.05, indicating that evapotranspiration from this permafrost black spruce forest was strongly coupled with ambient air. As a result, λE was mostly explained by evapotranspiration due to dryness of the air, $(1 - \Omega)\lambda E_{imp}$ (Fig. 12(c)).

At this site, g_a was 0.49 m s^{-1} at the mean value of summer (JJA, daytime). Considering the fact that g_a generally ranged from 0.05 to 0.1 on average and about 0.3 at maximum over five different boreal forests, cool-

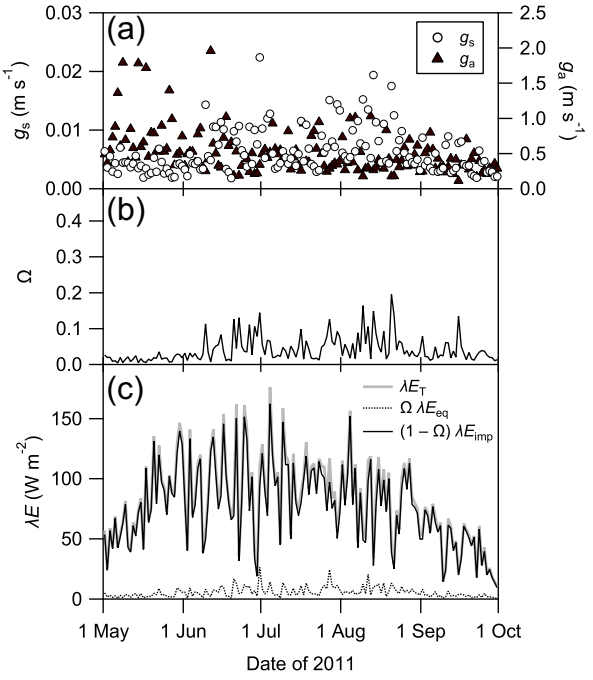

Fig. 12. Seasonal variations in (a) bulk surface conductance g_s and aerodynamic conductance g_a, (b) decoupling coefficient Ω, and (c) components of Eq. (9), i.e., λE, $\Omega\lambda E_{eq}$, and $(1-\Omega)\lambda E_{imp}$. These values were calculated from the daytime mean values from 11:00 to 15:00 AKST.

temperate and warm-temperate areas (Matsumoto et al., 2008b), the g_a of our site were exceptionally large. Though the stand density of this black spruce forest was relatively high (Table 1), the canopy height was low, and shoots were highly clumped on narrow tree crowns (see photos of Fig. 3). Therefore, the canopy structure of this black spruce forest was open, and considered aerodynamically rough, resulting in a high aerodynamic conductance g_a. On the other hand, g_s was 0.007 m s^{-1} at the mean value of summer (JJA, daytime), which was similar to that measured in larch and pine forests in eastern Siberia, 0.005–0.007 (Matsumoto et al., 2008b). Therefore, the small Ω in this forest was considered basically due to large g_a, indicating that the aerodynamically rough surface of this forest induced efficient turbulent transfer, and that ambient dry air was transferred effectively to the evaporating surface (forest floor and leaves of black spruce trees), resulting in well-coupled evapotranspiration with the ambient air.

4. Conclusions

We measured the evapotranspiration and energy budget in a permafrost black spruce forest in interior Alaska in 2011, and we examined the characteristics of evapotranspiration from this forest. The findings in this study are as follows.

1. Energy balance was nearly closed in summer, and the mean value of daily energy balance ratio over the summer (JJA) was 1.00. Ground heat flux played an important role in the daily energy balance in summer, accounting for 26.5% of net radiation. The large energy balance deficit was observed in spring, which was partly explained by the energy consumed during snowmelt within the limited period from 23 March to 1 May.
2. The mean daily evapotranspiration of this forest in summer was 1.37 mm day^{-1}, considered typical for boreal forests. The annual evapotranspiration and sublimation was 207.3 mm year^{-1}, which was much smaller than the annual precipitation, with 8.8% (18.2 mm year^{-1}) explained by sublimation.
3. The decoupling coefficient was generally small, and the mean value of summer (JJA, daytime) was 0.05, due to a large aerodynamic conductance over the aerodynamically rough surface of the black spruce forest. The evapotranspiration from this black spruce forest, therefore, was mostly explained by evapotranspiration due to the dryness of the air.

Acknowledgment

We thank Masahito Ueyama of Osaka Prefecture University for valuable comments, and Shiro Tsuyuzaki of Hokkaido University for identification of the forest floor vegetation at our site. We also acknowledge Nate Bauer of IARC, UAF for English proofreading of the manuscript, and two anonymous reviewers for their valuable comments. This research was conducted under the JAMSTEC-IARC Collaboration Study, with funding provided by the Japan Agency for Marine-Earth Science and Technology (JAMSTEC) under a grant to the International Arctic Research Center (IARC), and was also supported in part by the Japan Aerospace Exploration Agency (JAXA) in association with the IARC-JAXA Information System (IJIS).

References

Amiro, B., Wuschke, E., 1987. Evapotranspiration from a boreal forest drainage basin using an energy balance/eddy correlation technique. Boundary-Layer Meteorol. 38, 125–139.

Andreas, E., 2005. Handbook of Physical Constants and Functions for Use in Atmospheric Boundary Layer Studies. U.S. Army Cold Regions Research and Engineering Laboratory, Hanover, NH.

Baldocchi, D.D., Vogel, C.H., Brad, H., 1997. Seasonal variation of energy and water vapor exchange rates above and below a boreal jack pine forest canopy. J. Geophys. Res. 102, 28939−28951.

Billings, W.D., 1987. Carbon balance of Alaskan tundra and taiga ecosystems: past, present and future. Quat. Sci. Rev. 6, 165−177.

Bourgeau-Chavez, L.L., Garwood, G.C., Riordan, K., Koziol, B.W., Slawski, J., 2012. Development of calibration algorithms for selected water content reflectometry probes for burned and non-burned organic soils of Alaska. Int. J. Wildland Fire 19, 961−975.

Burba, G.G., McDermitt, D.K., Anderson, D.J., Furtaw, M.D., Eckles, R.D., 2010. Novel design of an enclosed CO_2/H_2O gas analyser for eddy covariance flux measurements. Tellus 62B, 743−748.

Burba, G.G., Schmidt, A., Scott, R.L., Nakai, T., Kathilankal, J., Fratini, G., Hanson, C., Law, B., McDermitt, D., Eckles, R., Furtaw, M., Velgersdyk, M., 2012. Calculating CO_2 and H_2O eddy covariance fluxes from an enclosed gas analyzer using an instantaneous mixing ratio. Glob. Change Biol. 18, 385−399.

Campbell Scientific, Inc., 2006. CS616 and CS625 Water Content Reflectometers Instruction Manual (Revision 8/06). Logan, UT.

Chapin III, F.S., Hollingsworth, T., Murray, D.F., Viereck, L.A., Walker, M.D., 2006. Floristic diversity and vegetation distribution in the Alaskan boreal forest. In: Chapin III, F.S., Oswood, M.W., Van Cleve, K., Viereck, L.A., Verbyla, D.L. (Eds.), Alaska's Changing Boreal Forest. Oxford University Press, New York, pp. 81−99.

Fitzjarrald, D., Moore, K., 1994. Growing season boundary layer climate and surface exchanges in a subarctic lichen woodland. J. Geophys. Res. 99, 1899−1917.

Fleagle, R., Businger, J., 1980. An Introduction to Atmospheric Physics, second ed. Academic Press, New York.

Fritschen, L., Gay, L., 1979. Environmental Instrumentation. Springer-Verlag, New York.

Hendricks Franssen, H.J., Stöckli, R., Lehner, I., Rotenberg, E., Seneviratne, S.I., 2010. Energy balance closure of eddy-covariance data: a multisite analysis for European FLUXNET stations. Agric. For. Meteorol. 150, 1553−1567.

Hinzman, L.D., Bettez, N.D., Bolton, W.R., Chapin, F.S., Dyurgerov, M.B., Fastie, C.L., Griffith, B., Hollister, R.D., Hope, A., Huntington, H.P., Jensen, A.M., Jia, G.J., Jorgenson, T., Kane, D.L., Klein, D.R., Kofinas, G., Lynch, A.H., Lloyd, A.H., McGuire, A.D., Nelson, F.E., Oechel, W.C., Osterkamp, T.E., Racine, C.H., Romanovsky, V.E., Stone, R.S., Stow, D.A., Sturm, M., Tweedie, C.E., Vourlitis, G.L., Walker, M.D., Walker, D.A., Webber, P.J., Welker, J.M., Winker, K.S., Yoshikawa, K., 2005. Evidence and implications of recent climate change in northern Alaska and other Arctic regions. Climatic Change 72, 251−298.

IPCC, 2001. Climate Change 2001: Impacts, Adaptation, and Vulnerability. In: Contribution of Working Group II to the Third Assessment Report of the Intergovernmental Panel on Climate Change. Cambridge University Press, New York.

Iwata, H., Harazono, Y., Ueyama, M., 2012. The role of permafrost in water exchange of a black spruce forest in interior Alaska. Agric. For. Meteorol. 161, 107−115.

Jarvis, P., Massheder, J., Hale, S., Moncrieff, J., Rayment, M., Scott, S., 1997. Seasonal variation of carbon dioxide, water vapor, and energy exchanges of a boreal black spruce forest. J. Geophys. Res. 102, 28953−28966.

Kelliher, F., Hollinger, D., Schulze, E.D., Vygodskaya, N., Byers, J., Hunt, J., McSeveny, T., Milukova, I., Sogatchev, A., Varlargin, A., Ziegler, W., Arneth, A., Bauer, G., 1997. Evaporation from an eastern Siberian larch forest. Agric. For. Meteorol. 85, 135−147.

Kormann, R., Meixner, F.X., 2001. An analytical footprint model for non-neutral stratification. Boundary-Layer Meteorol. 99, 207−224. http://dx.doi.org/10.1023/A:1018991015119.

Liu, H., Randerson, J.T., andand Lindfors, J., Chapin III, F., 2005. Changes in the surface energy budget after fire in boreal ecosystems of interior Alaska: an annual perspective. J. Geophys. Res. 110, D13101.

Matsumoto, K., Ohta, T., Nakai, T., Kuwada, T., Daikoku, K., Iida, S., Yabuki, H., Kononov, A.V., van der Molen, M.K., Kodama, Y., Maximov, T.C., Dolman, A.J., Hattori, S., 2008a. Energy consumption and evapotranspiration at several boreal and temperate forests in the far east. Agric. For. Meteorol. 148, 1978−1989.

Matsumoto, K., Ohta, T., Nakai, T., Kuwada, T., Daikoku, K., Iida, S., Yabuki, H., Kononov, A.V., van der Molen, M.K., Kodama, Y., Maximov, T.C., Dolman, A.J., Hattori, S., 2008b. Response of surface conductance to forest environments in the far east. Agric. For. Meteorol. 148, 1926−1940.

McMillen, R.T., 1988. An eddy correlation technique with extended applicability to non-simple terrain. Boundary-Layer Meteorol. 43, 231−245.

McNaughton, K.G., Jarvis, P.G., 1983. Predicting effects of vegetation changes on transpiration and evaporation. In: Kozlowski, T.T. (Ed.), 1983. Water Deficits and Plant Growth, vol. VII. Academic Press, New York, pp. 1−47.

Molotch, N., Blanken, P., Williams, M., Turnipseed, A., Monson, R., Margulis, S., 2007. Estimating sublimation of intercepted and sub-canopy snow using eddy covariance systems. Hydrol. Process. 21, 1567−1575.

Monteith, J.L., 1965. Evaporation and environment. Symp. Soc. Exp. Biol. 19, 205−224.

Moore, C.J., 1986. Frequency response corrections for eddy correlation systems. Boundary-Layer Meteorol. 37, 17−35.

Nakai, T., Iwata, H., Harazono, Y., 2011. Importance of mixing ratio for a long-term CO_2 flux measurement with a closed-path system. Tellus 63B, 302−308.

Nakai, T., Shimoyama, K., 2012. Ultrasonic anemometer angle of attack errors under turbulent conditions. Agric. For. Meteorol. 162−163, 14−26.

Nakai, T., Sumida, A., Kodama, Y., Hara, T., Ohta, T., 2010. A comparison between various definitions of forest stand height and aerodynamic canopy height. Agric. For. Meteorol. 150, 1225−1233.

Nakai, Y., Sakamoto, T., Terajima, T., Kitamura, K., Shirai, T., 1999. Energy balance above a boreal coniferous forest: a difference in turbulent fluxes between snow-covered and snow-free canopies. Hydrol. Process. 13, 515−529.

O'Donnell, J., Romanovsky, V., Harden, J., McGuire, A., 2009. The effect of moisture content on the thermal conductivity of moss and organic soil horizons from black spruce ecosystems in interior Alaska. Soil Sci. 174, 646−651.

Ohta, T., Hiyama, T., Tanaka, H., Kuwada, T., Maximov, T.C., Ohata, T., Fukushima, Y., 2001. Seasonal variation in the energy and water exchanges above and below a larch forest in eastern Siberia. Hydrol. Process. 15, 1459−1476.

Ohta, T., Maximov, T.C., Dolman, A.J., Nakai, T., van der Molen, M.K., Kononov, A.V., Maximov, A.P., Hiyama, T., Iijima, Y., Moors, E.J., Tanaka, H., Toba, T., Yabuki, H., 2008. Interannual variation of water balance and summer

evapotranspiration in an eastern Siberian larch forest over a 7-year period (1998−2006). Agric. For. Meteorol. 148, 1941−1953.

Reba, M.L., Pomeroy, J., Marks, D., Link, T., 2012. Estimating surface sublimation losses from snowpacks in a mountain catchment using eddy covariance and turbulent transfer calculations. Hydrol. Process. 26, 3699−3711.

Sauer, T., Akinyemi, O., Thery, P., Heitman, J., DeSutter, T., Horton, R., 2008. Evaluation of a new, perforated heat flux plate design. Int. Commun. Heat Mass. Transfer 35, 800−804.

Schotanus, P., Nieuwstadt, F.T.M., DeBruin, H.A.R., 1983. Temperature measurement with a sonic anemometer and its application to heat and moisture fluctuations. Boundary-Layer Meteorol. 26, 81−93.

Serreze, M., Walsh, J., Chapin, F.S.I., Osterkamp, T., Dyurgerov, M., Romanovsky, V., Oechel, W., Morison, J., Zhang, T., Barry, R., 2000. Observational evidence of recent change in the northern high-latitude environment. Climatic Change 46, 159−207.

Shuttleworth, W.J., Gurney, R.J., Hsu, A.Y., Ormsby, J.P., 1989. FIFE: The Variation in Energy Partition at Surface Flux Sites. IAHS Publ., p. 186.

Smith, W., Vissage, J., Darr, D., Sheffield, R., 2001. Forest Resources of the United States, 1997. Gen. Tech. Rep. NC-219. U.S. Department of Agriculture, Forest Service, North Central Research Station, St. Paul, MN.

Sugiura, K., Suzuki, R., Nakai, T., Busey, R.B., Hinzman, L.D., Park, H., Kim, Y., Nagai, S., Saito, K., Cherry, J.E., Ito, A., Ohata, T., Walsh, J., 2011. Supersite as a common platform for multi-observations in Alaska for a collaborative framework between JAMSTEC and IARC. JAMSTEC Rep. Res. Dev. 12, 61−69.

Ueyama, M., Hirata, R., Mano, M., Hamotani, K., Harazono, Y., Hirano, T., Miyata, A., Takagi, K., Takahashi, Y., 2012. Influences of various calculation options on heat, water and carbon fluxes determined by open- and closed-path eddy covariance methods. Tellus B 64.

Van Cleve, K., Dyrness, C.T., 1983. Introduction and overview of a multidisciplinary research project: the structure and function of a black spruce (*Picea mariana*) forest in relation to other fire-affected taiga ecosystems. Can. J. For. Res. 13, 695−702.

Vickers, D., Mahrt, L., 1997. Quality control and flux sampling problems for tower and aircraft data. J. Atmos. Oceanic Tech. 14, 512−526.

Viereck, L.A., Van Cleve, K., Dyrness, C.T., 1986. Forest ecosystem distribution in the taiga environment. In: Van Cleve, K., Chapin III, F.S., Flanagan, P.W., Viereck, L.A., Dyrness, C.T. (Eds.), Forest Ecosystems in the Alaskan Taiga. Springer-Verlag, New York, pp. 22−43.

Whittaker, R.H., 1975. Communities and Ecosystems, second ed. Macmillan, New York.